Modeling and Time-Optimal Control of an Experimental Hybrid Dynamic System

Hainan Wang[1] and Edward P. Gatzke[1*]

[1]Department of Chemical Engineering, University of South Carolina, Columbia, SC

[*]Corresponding Author gatzke@sc.edu (803) 777-1159

Short Title: Modeling & Control of an Experimental Hybrid Sys.

Modeling and Time-Optimal Control of an Experimental Hybrid Dynamic System

Abstract

Optimization of hybrid dynamic systems typically involves characterizing switching times and mode sequences. Operating autonomous hybrid systems with varying event timings presents multiple challenges. Complexity often arises from optimal mode sequence determination, making optimization of the corresponding hybrid automaton more difficult. An experimental autonomous hybrid dynamic system experiencing switching due to choked flow conditions is presented. Implementing gradient-based optimization algorithms may be difficult due to complex switching patterns of the hybrid dynamic systems. To mitigate this, an approximation of the Heaviside step function is applied to transform the hybrid switching functions to a continuous and smooth forms. Using the Control Vector Parameterization (CVP) approach and evaluating gradients using the variational method, an open-loop time-optimal control problem is presented. Modeling and control methods are demonstrated using an experimental two-tank air system. The optimal control formulation can include constraints to avoid specific undesirable modes of operation.

Index

i: index of control variables

j: index of equality/inequality constraints

k: index of time intervals

l: dummy index for sensitivity equations

m: index of mode

q: index of epochs

m_q: index of mode at epoch q

Symbol

n_m: total number of nodes

n_e: total number of epochs

n_1: total number of inequality path constraints

n_2: total number of terminal equality constraints

1 Introduction

Constrained dynamic Optimal Control Problems (OCPs) have received extensive theoretical investigation.[1,2] In many systems, the governing equations used to model continuous dynamic systems remain consistent across the entire time horizon. However, the emergence of discontinuities stemming from phase changes, flow transitions/reversals, irregularities in process vessel geometry, and external control actions can introduce complexities in process modeling and optimization. These phenomena are frequently modeled as sudden alterations to the subsystem governing the process of interest. Each individual subsystem type is referred to as a mode or state.[3] The comprehensive system describing the complete engineering process consists of multiple such modes which form a sequence known as the hybrid mode sequence.[3] The progression of the system at specific time points is commonly described as the process event timings. These events are typically triggered when the system fulfills specific transition conditions, often linked to transition functions that outline the transition. Dynamic systems with abrupt changes are commonly called hybrid dynamic systems.

The theoretical and practical significance of hybrid systems stems from their wide range of applications which reflect the complexity of the real world. In the field of industrial automation, hybrid systems can manage and optimize production processes, achieving a seamless interface between material handling and machine operation.[4] Energy management systems also use the concept of hybrid systems to balance load and generating capacity to respond to instantaneous changes in the electrical grid.[5] In intelligent transportation systems, hybrid systems can handle the continuous and discrete aspects of vehicle dynamics, thereby improving energy efficiency.[6] In biomedical engineering, hybrid systems are used to model the complex processes of cell growth within bioreactors as well as the effects of discrete fed-batch systems.[7] These applications indicate that hybrid systems are crucial for modern science and engineering because they provide tools for analyzing and designing complex, multi-scale, and interdisciplinary systems.

Researchers established a comprehensive framework to understand and encompass these complex systems. This framework aims to integrate advanced mathematical theories with practical engineering techniques, thus providing a systematic approach for analyzing, designing, and optimizing hybrid systems: Barton and Pantelides[8] proposed a general modeling framework for discrete/continuous processing systems operating in the continuous time domain. Bemporad and Morari[9] presented a framework for systematic design of modeling and optimal control of linear and mixed-integer linear programming and demonstrated on a gas supply system. DeCarlo et al.[10] presented general theorems for nonlinear hybrid systems and results for verification of stability of hybrid systems applied in automotive controls and avionics. Frequent exhibition of hybrid characteristic in real applications motivates the development of modeling framework: Alur et al.[11,12] suggested the hybrid systems were best analyzed within a hybrid automaton framework, which suggested each state should be characterized additionally by a set of variables and equations describing the system in that state. Dimitriadis et al.[13] proposed a modified framework within which purely discrete, purely continuous and hybrid systems of arbitrary complexity can be constructed consistently and then incorporated into a safety verification problem. Later, Feehery and Barton[14–16] enriched the methodology on hybrid dynamic models by formulating a broad class of hybrid discrete/continuous phenomena, presenting insight on sensitivity analysis of a hybrid system and progress on optimization procedures. Parametric sensitivity analysis, concerned with the sensitivity of the predicted model to infinitesimal perturbations in parameters, had many applications in parameter estimation and optimization for hybrid systems.[16,17]

Research on developing deterministic algorithms for global solution of hybrid dynamic optimization problems attracted interest due to a need to devise robust methods for automated design.[3,18] Within a general hybrid framework based on continuous hybrid automaton and depending on characteristic of the optimization problem formulation, a classification of optimization problems of hybrid system embedded as well as solving approaches was attempted to provide as in the work by Barton et al.[3] In summary, hybrid system theory

includes modeling with an emphasis on exposing the discontinuity, developing suitable algorithms on identifying the model with exact switching conditions and optimal parameters, and performing optimal control. The optimization of hybrid dynamic problems is typically associated with optimal mode sequence decisions.

In previous work,[19] the nonlinear behavior and complex dynamics of the air flow behavior in a tank system presents an interesting problem with switching dynamics. One goal of the present work is to develop a high-fidelity model with available experimental data in order to simulate the air flow behavior in tank system. A generalized model of coupled nonlinear ordinary differential equations is presented. Using data collected from the experimental apparatus, parameter estimation is achieved with MATLAB/Simulink. The proposed model with estimated model parameters provides a basis for an open-loop optimal control problem. The problem is solved with constraints enforced to avoid specified modes of operation. The optimization results are then demonstrated experimentally.

With respect to open-loop control of the proposed hybrid system, a similar hybrid system due to choked flow is found in previous work[15] where the control signals are binary values. The corresponding optimization formulation is a Mixed Integer Non-Linear Programming (MINLP) problem. Distinctively, the current experimental multi-variable pressure tank system accepts user-specified piece-wise constant control signal. Within the framework based on hybrid automaton and by classification of Barton,[3] the optimization problem formulation of the proposed hybrid system uses nonlinear functions, varying event timings, and an autonomous mode sequence. A possible solution approach could be based on a nonconvex MINLP formulation.[3]

In the current work, the determination of event timings and mode sequences are uniquely determined by the control input. Directly applying a Control Vector Parameterizaton (CVP) algorithm to the OCP of proposed system requires the determination of event timings and mode sequence a priori for a specific control. This is not easily attainable and can lead to poor convergence using NLP optimization. This issue is addressed by introducing a

smoothed Heaviside function[20] to represent all modes and ensure only one mode is exclusively active. The solutions of the proposed OCP with hybrid dynamics could be used for solution of engineering tasks such as safety verification. Additionally, optimal process start-up/shutdown/transition could be considered for choked flow systems. This work could be extended to other binary hybrid systems.

This work is structured as follows: The modified hybrid framework is presented in Section 2. Section 3 describes the proposed hybrid model and proposed CVP method: In Section 3.1 a hybrid dynamic model is built due to choked flow phenomenon in gas transportation which provides the base for the control problem. A standard estimation routine is applied to estimate model parameters from experiment data in Section 3.2. In Section 4, an illustrative OCP of proposed hybrid system is posed and a CVP-based algorithm with gradient evaluated by trajectory sensitivity is implemented to solve hybrid time-optimal OCP. Results are presented and discussed in Section 5 with conclusions in Section 6.

2 Background and Problem Formulation

Consider a dynamic system described by following first-order Ordinary Differential Equation (ODE) defined on $[t_0, t_F]$:

$$\dot{\boldsymbol{x}}(t) = \hat{\boldsymbol{f}}(\boldsymbol{x}(t), \hat{\boldsymbol{u}}(t), \boldsymbol{p}) \tag{1}$$
$$\boldsymbol{x}(t_0) = \boldsymbol{x}_0 \tag{2}$$

Here, t_0 is the given initial time, t_F is the terminal time ($t_F > t_0$), $\boldsymbol{x}(t) \in \mathbb{R}^{n_x}$ are the state variables, $\hat{\boldsymbol{u}}(t) \in \mathbb{R}^{n_u}$ are the continuous control variables, $\boldsymbol{p} \in \mathbb{R}^{n_p}$ is the vector of time-invariant parameters, $\boldsymbol{x}_0$ is the given initial states, and $\hat{\boldsymbol{f}} : \mathbb{R}^{n_x} \times \mathbb{R}^{n_u} \times \mathbb{R}^{n_p} \to \mathbb{R}^{n_x}$ is the vector function assuming continuously differentiable with respect to all arguments.

In practical applications, continuous control variables are often discretized, thereby transforming the infinite-dimensional OCP into a finite-dimensional one. The two most popular discretization policies are piecewise constant and piecewise linear which correspond to the

forms of first-order and second-order basis functions of the B-spline function, respectively.[21] The experimental setup for this study is designed to accept piecewise constant signals, which is also the most commonly used form of discretization policy. Therefore, the entire time horizon $t \in [t_0, t_F]$ is divided by switching time nodes t_k into N time intervals:

$$[t_0, t_F] = [t_0, t_1) \cup [t_1, t_2) \cup ... \cup [t_{N-1}, t_N] \tag{3}$$

where $t_N = t_F$. Each control variable $\hat{u}_i$ of $\hat{\boldsymbol{u}}(t)$ is approximated as time-invariant control values $\sigma_{i,k}$ on k^{th} time intervals:

$$\hat{u}_i(t) \approx u_i(t) = \sum_{k=1}^{N} \sigma_{i,k} \chi_{[t_{k-1}, t_k)}(t), i = 1, ..., n_u, k = 1, ..., N \tag{4}$$

where $\chi_I(t)$ is the first-order basis function of B-spline function which is also called the indicator function:

$$\chi_I(t) = \begin{cases} 1, & \text{if } t \in I \\ 0, & \text{if } t \notin I \end{cases} \tag{5}$$

The control values $\sigma_{i,k}$ taken in the same k^{th} stage is defined as the control value vector $\boldsymbol{\sigma}_k$.

$$\boldsymbol{\sigma}_k = [\sigma_{1,k}, ..., \sigma_{n_u,k}]^T \in \mathbb{R}^{n_u}, k = 1, ..., N \tag{6}$$

The overall control value vector $\boldsymbol{\sigma}$ contains all $\boldsymbol{\sigma}_k$ vectors:

$$\boldsymbol{\sigma} = \left[\boldsymbol{\sigma}_1^T, ..., \boldsymbol{\sigma}_N^T\right]^T = \left[\sigma_{1,1}, ..., \sigma_{n_u,1}, \sigma_{1,2}, ..., \sigma_{n_u,2}, ..., \sigma_{1,N}, ..., \sigma_{n_u,N}\right]^T \in \mathbb{R}^{n_u \times N} \tag{7}$$

A set of switching times $\boldsymbol{t}$ is defined as:

$$T = \left\{ \boldsymbol{t} = \left[t_1, ..., t_N \left(= t_F\right)\right]^T \in \mathbb{R}^N : t_{k-1} < t_k, k = 1, ..., N \right\} \tag{8}$$

The difference of two adjacent switching time nodes is denoted as the time interval length $\delta_k = t_k - t_{k-1}$. The vector of time interval lengths is denoted as $\boldsymbol{\delta}$:

$$\boldsymbol{\delta} = \left[\delta_1, ..., \delta_N\right]^T \in \mathbb{R}^N \tag{9}$$

Using control vector parameterization of eq 1, a non-hybrid dynamic system with discretized control is rewritten as:

$$\dot{\boldsymbol{x}}\left(t\right) = \boldsymbol{f}\left(\boldsymbol{x}\left(t|\boldsymbol{\sigma}, \boldsymbol{p}, \boldsymbol{t}\right), \boldsymbol{u}\left(t|\boldsymbol{\sigma}, \boldsymbol{t}\right), \boldsymbol{p}\right) \tag{10}$$

$$\boldsymbol{x}\left(t_0\right) = \boldsymbol{x}_0 \tag{11}$$

In the context of a hybrid dynamic system, formulating the problem becomes more complex. The hybrid system framework introduced by Barton et al.[3] is presented here. This original framework serves as a suitable modeling paradigm for coupled continuous state and discrete state dynamics of embedded hybrid systems. In order to accommodate the autonomous hybrid model proposed in this study, only limited modifications have been made.

At the core of this framework lies the hybrid automaton, comprising discrete modes,

decision variables, state variables, dynamics of each mode, mode transitions, and transition functions.[3] When describing the dynamic evolution of a hybrid system within this framework, it is divided into two parts: The dynamics within each mode and the transitions between modes. Discrete modes are discrete states of hybrid automation. At time points other than transition, the system permits the existence of only one mode which is referred to as the active mode.[3] There should be a finite number of modes and a finite index set of all modes $M = \{1, 2, ..., n_m\}$ where n_m is the total number of modes.

A continuous system describing the dynamic of each mode $m \in M$ which is characterized by a system of nonlinear ODEs governing the evolution of the state variables when mode m_q is the current active mode is given as:

$$\dot{\boldsymbol{x}}(t) = \sum_{q=1}^{n_e} \boldsymbol{f}^{(m_q)}\left(\boldsymbol{x}\left(t|\boldsymbol{\sigma}, \boldsymbol{p}, \boldsymbol{t}\right), \boldsymbol{u}\left(t|\boldsymbol{\sigma}, \boldsymbol{t}\right), \boldsymbol{p}\right) \chi_{[\tau_{q-1}, \tau_q)}(t) \tag{12}$$

The time horizon is divided into consecutive intervals known as epochs I_q, where each epoch represents a time interval:

$$I_q = [\tau_{q-1}, \tau_q) \subset \mathbb{R} \tag{13}$$

with $\tau_{q-1} \leq \tau_q$, $q = 1, ..., n_e$. The hybrid time trajectory T_τ, is a finite sequence of epoch $\{I_q\}$ and n_e is the total number of epochs. Corresponding to the sequence of epochs is a finite sequence of modes, hybrid mode trajectory T_μ is a sequence:

$$T_\mu = m_1, ..., m_{n_e} \tag{14}$$

with $m_q \in M$, $q = 1, ..., n_e$. Any mode may be visited multiple times in this sequence. For each epoch I_q, the discrete state of the hybrid automaton is mode m_q and a transition to a new mode m_{q+1} takes place at τ_q.

A transition may be controlled or autonomous. A controlled transition occurs at a certain time in direct response to a control action. An autonomous transition occurs whenever a

transition condition involving state variables, parameters and time become satisfied. A common formulation for transition conditions is taking the transition at the earliest time τ_q at which a discontinuity function, $g\left(\boldsymbol{x}\left(t|\boldsymbol{\sigma},\boldsymbol{p},\boldsymbol{t}\right),\boldsymbol{u}\left(t|\boldsymbol{\sigma},\boldsymbol{t}\right),\boldsymbol{p}\right)$, crosses zero.

The vector of decision variables, denoted as $\boldsymbol{z} \in \mathbb{R}^{n_z}$, can be categorized into three classes of variables based on the inclusion of variable switching times and the presence of model parameters to be determined. Taking into account both variable switching times and model parameters, the vector $\boldsymbol{z}$ is formulated as $\boldsymbol{z}^T = \left[\boldsymbol{\sigma}^T, \boldsymbol{p}^T, \boldsymbol{t}^T\right]^T$.

Regardless of either controlled or autonomous transition, the transition condition can be represented as a common formulation:

$$\boldsymbol{x}\left(\tau_{q+1}—\boldsymbol{z}\right) = \boldsymbol{T}\left(\boldsymbol{x}\left(\tau_q—\boldsymbol{z}\right),\boldsymbol{z},\tau_q\right) \tag{15}$$

where τ_q is the time at which the transition occurs. The simplest and most common transition function is state continuity:

$$\boldsymbol{x}\left(\tau_{q+1}|\boldsymbol{z}\right) = \boldsymbol{x}\left(\tau_q|\boldsymbol{z}\right) \tag{16}$$

Given values of decision variables $\boldsymbol{z}$, a simulation or execution of the hybrid automaton is characterized by epochs, mode trajectory, initial mode and initial condition. The initial mode m_1 and the initial condition,

$$\boldsymbol{x}\left(t_0 = \tau_0\right) = \boldsymbol{x}_0 \tag{17}$$

both may be decisions to be made by the optimization.

3 Tank Model and Parameter Estimation

In this section, the experimental hybrid model arising from choked flow phenomenon in a gas tank system is presented. Subsection 3.1 introduces the experimental setup and modeling while subsection 3.2 describes the process of parameter optimization using a conventional

parameter estimation method.

3.1 Experimental Setup and Modeling

In this subsection, an experimental process model derived from a multivariable pressure tank system is presented based on fundamental principles.[19] This nonlinear hybrid dynamic model depicts the air flow dynamics within an experimental system encompassing tanks, pipes, and valves. The actual experimental apparatus consists of four interconnected air tanks, allowing configuration changes through valve manipulation.

Specifically, a two-tank configuration in series has been designed in current study as depicted in Figure 1. At $t = 0$, high pressure air is feed into tank system and sequentially flows through control valve CV_1, followed by needle valves V_{12} and V_{22}. The needle valves V_{12} and V_{22} are partially open. The LabVIEW interface enables adjustment of the opening percentage allowing for piecewise constant input control policies. Sensors of Tank 3 and Tank 4 act as surrogates to measure the feed pressure P_0 and the atmosphere pressure P_3 respectively.

Assuming isothermal operation and applicability of the ideal gas law $P_i(t) = n_i(t)\,RT$, the coupled balance equations for the configuration in terms of tank pressures are derived as follows:

$$\begin{aligned} \frac{V_1}{RT}\frac{dP_1(t)}{dt} &= N_1(t) - N_2(t) \\ \frac{V_2}{RT}\frac{dP_2(t)}{dt} &= N_2(t) - N_3(t) \end{aligned} \tag{18}$$

where N_1 represents the molar flow rate across CV_1, while N_2 and N_3 denote the molar flow rates across V_{12} and V_{22}, respectively.

This hybrid dynamic model stems from the physical phenomenon of transitions between

normal and choked flow regimes. Choked flow is a pivotal condition where the mass flow through a constraints reaches a point beyond which further reducing downstream pressure does not increase the mass flow rate.[22,23] The effects of choked flow are seen in the transition of flow rate across valves between normal laminar/turbulent flow and choked regime.

The occurrence of this transition autonomously arises when the upstream/downstream pressure ratio of a particular valve crosses a threshold.[24,25] The molar flow rates are defined as functions of dynamic state variables such as upstream/downstream pressures, control variables such as control valve open-up percentage, and other time-invariant model parameters related to valve characteristics and thermodynamic properties.[19]

The hybrid dynamic model entails distinct flow rate expressions. These expressions correspond to the choked flow condition $P_{i-1}/P_i \geq 2$, or the normal flow condition $2 \geq P_{i-1}/P_i, i = 1, 2, 3$. Note $P_{i-1}/P_i > 1$ implies no reverse flow across the valve. For those valves, the continuous molar flow rates N_i, $i = 1, 2, 3$ are given as:[24,25]

$$
\begin{aligned}
N_1 &= \begin{cases} k_1 \Gamma^{x_3 - 1} \sqrt{P_0^2/2} & \text{if } P_0/P_1 \geq 2 \\ k_1 \Gamma^{x_3 - 1} \sqrt{P_0 \left(P_0 - P_1\right)} & \text{if } 2 \geq P_0/P_1 \geq 1 \\ 0 & \text{if } P_0/P_1 \leq 1 \end{cases} \\
N_2 &= \begin{cases} 0.471 k_2 P_1 & \text{if } P_1/P_2 \geq 2 \\ k_2 \left(1 - 2\left(P_1 - P_2\right)/3P_1\right) \sqrt{P_1 \left(P_1 - P_2\right)} & \text{if } 2 \geq P_1/P_2 \geq 1 \\ 0 & \text{if } P_1/P_2 \leq 1 \end{cases} \\
N_3 &= \begin{cases} 0.471 k_3 P_2 & \text{if } P_2/P_3 \geq 2 \\ k_3 \left(1 - 2\left(P_1 - P_2\right)/3P_1\right) \sqrt{P_2 \left(P_2 - P_3\right)} & \text{if } 2 \geq P_2/P_3 \geq 1 \\ 0 & \text{if } P_2/P_3 \leq 1 \end{cases}
\end{aligned} \tag{19}
$$

Acknowledging that the valve position switch for CV_1 does not occur instantaneously, it is assumed that the control signal u_1 with in the range $[0, 100\%]$ is subjected to low-pass filtering with a time constant τ_m. This leads to the following model equations where the V_1/RT and V_2/RT are consolidated as characteristic volume constants V_{1e} and V_{2e}:

Table 1: Model parameters of hybrid system capturing switching behavior

Variable name	Symbol	Unit
Valve coefficient for CV_1	k_1	$\text{in}^3\,\text{mol}/\,\text{J}$
Valve coefficient for valve V_{12}	k_2	$\text{in}^3\,\text{mol}/\,\text{J}$
Valve coefficient for valve V_{22}	k_3	$\text{in}^3\,\text{mol}/\,\text{J}$
Characteristic volume constant of tank 1	V_{1e}	mol/psi
Characteristic volume constant of tank 2	V_{2e}	mol/psi
Actuator dynamic time constant	τ_m	1
Base of the exponential lift function	Γ	1

$$
\begin{aligned}
\dot{x_1} &= \dot{P_1} = (N_1 - N_2)\,/V_{1e} \\
\dot{x_2} &= \dot{P_2} = (N_2 - N_3)\,/V_{2e} \\
\dot{x_3} &= (-x_3 + u_1)\,/\tau_m
\end{aligned} \tag{20}
$$

The model parameters presented in Table 2 will be estimated using nonlinear regression based on the dynamic model in Subsection 3.2.

3.2 Parameter Estimation

A set of discretely sampled data for $P_{1\text{m}}$ and $P_{2\text{m}}$ was acquired at a discrete sampling time-series $\boldsymbol{t}_n$ from the experimental setup. The system was driven by user-specified piece-wise constant control inputs as illustrated in Figure 2. The estimation of parameters for the hybrid model can be framed as an optimization problem which minimizes the sum squared errors arising from the disparities between the simulated and measured state variables P_1 and P_2:

$$\min_{\boldsymbol{p}} \sum_{n=1}^{n_y} \left(\left(P_{1\mathrm{m}}\left(t_n|\boldsymbol{\sigma},\boldsymbol{p},\boldsymbol{t}\right) - P_{1\mathrm{s}}\left(t_n|\boldsymbol{\sigma},\boldsymbol{p},\boldsymbol{t}\right)\right)^2 + \left(P_{2\mathrm{m}}\left(t_n|\boldsymbol{\sigma},\boldsymbol{p},\boldsymbol{t}\right) - P_{2\mathrm{s}}\left(t_n|\boldsymbol{\sigma},\boldsymbol{p},\boldsymbol{t}\right)\right)^2 \right)$$

$s.t.$

$$\begin{aligned} \dot{\boldsymbol{x}}\left(t\right) &= \boldsymbol{f}^{(m_q)}\left(\boldsymbol{x}\left(t|\boldsymbol{\sigma},\boldsymbol{p},\boldsymbol{t}\right),\boldsymbol{u}\left(t|\boldsymbol{\sigma},\boldsymbol{t}\right),\boldsymbol{p}\right), \forall t \in \left[\tau_{q-1},\tau_q\right) \\ \boldsymbol{y}\left(t_n\right) &= \begin{bmatrix} P_{1\mathrm{m}}\ \left(t_n\right) & P_{2\mathrm{m}}\left(t_n\right) \end{bmatrix}^T \end{aligned} \tag{21}$$

where $\boldsymbol{p} \in \mathbb{R}^{n_p}$ is the vector of model parameters to be optimized with their specific definitions as defined in Table 1. The time points t_n denote the sampling time points and n_y is the total number of data points available. The quantities $P_{1\mathrm{m}}$ and $P_{2\mathrm{m}}$ represent the measured states as visually depicted in Figure 2. The quantities $P_{1\mathrm{s}}$ and $P_{2\mathrm{s}}$ correspond to the simulated state trajectories derived from eqs 20 and 19. The data array $\boldsymbol{y}$ represents discrete measured variables, encompassing $P_{1\mathrm{m}}$ and $P_{2\mathrm{m}}$.

One may notice that the measured feed pressure $P_{0\mathrm{m}}$ and the atmospheric pressure $P_{3\mathrm{m}}$ are not constant in the experimental data. The supply pressure $P_{0\mathrm{m}}$ fluctuates whenever the valve position switches as depicted in Figure 3. To obtain accurate model parameters, the hybrid model was developed in MATLAB/Simulink and solved by a standard optimization routine with gradient evaluated by finite difference method. The resulting optimal model parameters are documented in Table 2. The corresponding simulated $P_{1\mathrm{s}}$ and $P_{2\mathrm{s}}$ values and the simulated/measured discrepancies are depicted in Figure 4. The hybrid dynamic model using the estimated model parameters will act as the model system for the optimization problem detailed in Section 4. Figure 5 shows the phase plane $P_{1\mathrm{m}}\left(t\right)$ versus $P_{2\mathrm{m}}\left(t\right)$ for the system, including the boundaries between operation modes.

Table 2: Estimated model parameters of hybrid system

Variable Name	Final	Lower/Upper bound	Gradient at J^*
k_1	18.1119	$(0, 30)$	-0.0024
k_2	1.8046	$(0, 3)$	-0.0273
k_3	2.0703	$(0, 3)$	0.0129
V_{1e}	21.0940	$(18.686, 22.838)$	-0.0018
V_{2e}	5.8173	$(5.189, 6.667)$	-0.0069
τ_m	0.8897	$(0, 2)$	-0.0026
R	85.1522	$(50, 200)$	0.0005

ode45 tolerance AbsTol = RelTol = 10^{-12}
fmincon tolerance TolX = TolFun = 10^{-8}

4 Problem Formulation and Solution

In Subsection 4.1, the construction of an optimization problem with path constraints is discussed, along with discussions of the challenges arising during optimization due to the distinctive attributes of the hybrid model. In subsection 4.2, the challenges posed by the hybrid model are presented, along with the smoothed Heaviside step function which overcomes some numerical difficulties. Subsection 4.3 introduces the variational method for solution of the stated optimization problem, accompanied by the derivations of corresponding sensitivity and gradient formulas.

Given the estimation of model parameters $\boldsymbol{p}$ in Section 3, an assumption can be made that these parameters remain unchanged throughout the simulation process. Consequently, $\boldsymbol{x}\left(t|\boldsymbol{\sigma}, \boldsymbol{p}, \boldsymbol{t}\right)$ will henceforth be represented as $\boldsymbol{x}\left(t|\boldsymbol{\sigma}, \boldsymbol{t}\right)$. In contexts devoid of ambiguity, the symbols $\boldsymbol{x}\left(t|\boldsymbol{\sigma}, \boldsymbol{t}\right)$ and $\boldsymbol{u}\left(t|\boldsymbol{\sigma}, \boldsymbol{t}\right)$ can be further simplified to $\boldsymbol{x}\left(t\right)$ and $\boldsymbol{f}\left(\boldsymbol{x}\left(t\right), \boldsymbol{u}\left(t\right)\right)$.

4.1 Problem Formulation

The vector of model parameters denoted by $\boldsymbol{p}$ was defined. This hybrid model with the estimated parameters $\boldsymbol{p}$ serves as a foundation for optimal control of the system. For corre-

sponding optimization problems, the decision variables that need to be determined includes the control values $\boldsymbol{\sigma}$ as well as the switching times $\boldsymbol{t}$. The determination of times $\boldsymbol{t}$ is equivalent to determination of duration of variable time intervals $\boldsymbol{\delta}$. A time-optimal control problem with state path constraint G_1 and terminal point constraint $\boldsymbol{x}(t_F) = \boldsymbol{x}_F$ is considered in the present work:

Problem 1

$$
\begin{aligned}
&\min_{\boldsymbol{\sigma},\boldsymbol{t}} J = t_F \\
s.t.& \\
&\dot{x_1} = \dot{P}_1 = (N_1 - N_2)/V_{1e} \\
&\dot{x_2} = \dot{P}_2 = (N_2 - N_3)/V_{2e} \\
&\dot{x_3} = (-x_3 + u_1)/\tau_m \\
&\forall t \in [\tau_{q-1}, \tau_q), q = 1, ..., n_e \\
&\boldsymbol{x}(t_0) = \boldsymbol{x}_0 \\
&\boldsymbol{x}(t_F) = \boldsymbol{x}_F \\
&G_1 = P_1 - 1.5P_2 \leq 0
\end{aligned} \tag{22}
$$

where the molar flow rates N_1, N_2, and N_3 in Problem 1 refer to their definitions in eq 19. Problem 1 is an illustrative hybrid time-optimal control problem simulating a start-up process with path constraints avoiding undesirable phase plane regions. The tank apparatus is to be transitioned from a specified initial state $\boldsymbol{x}_0 = \boldsymbol{x}(t = 0)$ to another terminal state at $\boldsymbol{x}(t = t_F)$ by an admissible control policy which minimizes the transition time. To enhance the realism and complexity of the optimization problem, a path constraint, $P_1 \leq 1.5P_2$, is added to the problem. The significance of this path constraint lies its role in guaranteeing that the selected valve operates within the constrained pressure ratio. This avoids any pressure drops leading to choked flow, a phenomenon which can potentially have detrimental

effects on both the valve and the pipe. These effects include vibrations linked to excessive noise, equipment wear, and challenges in operation.

A similar tank changeover example was studied in the previous work where the path constraint was introduced to avoid the formation of an explosive composition mixture in the vessel at any time during the changeover[15]. In the explored tank changeover problem,[15] the valves are assumed to be fully opened or completely closed leading to binary variables into optimization formulation. The optimization problems associated with hybrid systems can be categorized into various classes. This classification is contingent upon factors such as the Linear Time-Varying (LTV) or nonlinear system dynamics, whether functionals are affine or nonlinear, whether fixed or varying event timings, and whether mode sequence is fixed/unfixed or switches controlled/autonomous.[3] By classification of various kind of hybrid optimal problem,[3] the tank changeover example is classified as a nonsmooth MINLP (Mixed-Integer Nonlinear Programming) optimization problem with varying event timings and autonomous mode sequence and was solved with an Integrated Controlled Random Search (ICRS) MINLP approach.[15,26] In the problem studied in this work, the valve position is controllable $u_1 \in [0, 100\%]$. Therefore, based on classification, the optimization problem Problem 1 should fall under the category of a MINLP optimization with varying event timings and autonomous mode sequence. In the following section, challenges in directly solving this optimization problem will be highlighted, and the method of approximating this MINLP problem as a NLP problem using a smoothed Heaviside step function will be introduced. This approach aims to enhance the efficiency and stability of the solution process, enabling more flexible management of hybrid system switchings in practical applications.

4.2 Smoothed Heaviside Step Function

For any given input sequences defined by control values $\boldsymbol{\sigma}$ and switching time points $\boldsymbol{t}$, the execution of the hybrid automaton with dynamics described in Problem 1 is characterized

by the finite sequence of epochs and the corresponding mode sequence which needs to be determined a priori. For the hybrid gas-flow system with choked flow, autonomous transitions occur whenever the transition condition $g\left(\boldsymbol{x}\left(t|\boldsymbol{\sigma},\boldsymbol{t}\right),\boldsymbol{u}\left(t|\boldsymbol{\sigma},\boldsymbol{t}\right)\right)$ is met.

The determination of event timings τ_{q-1}/τ_q for a given $(\boldsymbol{\sigma},\boldsymbol{t})$ decides the hybrid time trajectory T_τ and corresponding hybrid mode trajectory T_μ. This could be clearly depicted in the two-dimensional phase plane, where the sampled data points $P_{1\mathrm{m}}$ and $P_{2\mathrm{m}}$ are portrayed on the phase plane. Given that reverse flow is not permitted, the trajectory can only exist in the upper-left region, indicating $P_0 > P_1 > P_2 > P_{\mathrm{atm}}$. Within this region, three threshold curves on the phase plane indicate the threshold values of the upstream to downstream ratios necessary for occurrence of choked flow. These three threshold curves partition the upper-left area into several distinct regions labeled as A to G in Figure 5 with each representing one mode m_q. Regions A to G show the different region of modes of operation. One may notice that the boundaries between certain mode regions are defined only by a common geometric point, such as the common point between regions A and C. Theoretically, a transition from mode A to C through this common point is feasible, although a dual-mode simultaneous transition is extremely challenging to implement from an experimental perspective.

Event timings τ_{q-1} and τ_q are marked by the time points when state trajectory intersects the boundaries of these regions. The sequence of state trajectory passing through those regions forms the mode trajectory T_μ. A continuous-time hybrid automaton, presented in Figure 6, explicitly illustrates all potential individual transitions between adjacent mode regions of phase plane, as depicted in Figure 5.

However, it is difficult to determine the exact event times given the state equations and the specified control policies input dependent on user-specified $(\boldsymbol{\sigma},\boldsymbol{t})$. A natural approach to simplify the problem is to introduce binary variables y_{mq} for all modes $m = 1, ..., n_m$ and all epochs $q = 1, ..., n_e$:[3]

$$\dot{\boldsymbol{x}}\left(t\right) = \sum_{m=1}^{n_m} y_{mq} \boldsymbol{f}^{(m_q)}\left(\boldsymbol{x}\left(t|\boldsymbol{\sigma},\boldsymbol{t}\right),\boldsymbol{u}\left(t|\boldsymbol{\sigma},\boldsymbol{t}\right)\right), \forall t \in \left[\tau_{q-1},\tau_q\right) \tag{23}$$

The binary variable y_{mq} is set to 1 if mode m is active during epoch q and it is set to 0 if mode m is inactive during that epoch q. The inclusion of the allocation constraint ensures that exactly one mode is active in each epoch:

$$\sum_{m=1}^{n_m} y_{mq} = 1, \forall q = 1, ..., n_e \tag{24}$$

Rather than enumerating all modes of the hybrid dynamic system, binary variables can be used to switch the lower level equations (19) defining the flow rates. For a piecewise system containing only two subsystems, it is straightforward to use the Heaviside step function to represent the discontinuity. A smooth approximation of the Heaviside step function,[20] using the transition condition $g(\boldsymbol{x}, \boldsymbol{u})$ as the independent variable, is defined as:

$$H(g(\boldsymbol{x}, \boldsymbol{u})) = H_1\{g(\boldsymbol{x}, \boldsymbol{u}), \lambda\}|_{\lambda\to\infty} = \lim_{\lambda\to\infty} arctan(\lambda g(\boldsymbol{x}, \boldsymbol{u}))/\pi + 1/2 \tag{25}$$

For readability, the two arguments $g(\boldsymbol{x}, \boldsymbol{u})$ and λ in smoothed penalty function $H_1\{\cdot\}$ are enclosed in braces $\{\cdot\}$ in the following context. The graph showing λ values ranging from 1 to 500 is depicted in Figure 7.

The piecewise molar flow rate expressions N_1, N_2, and N_3, as outlined in (19) can be transitioned into a continuous function by using the aforementioned smooth Heaviside function (25). This results in the integrated flow rate expressions N_1^H, N_2^H, and N_3^H:

$$\begin{aligned}
N_1^H =& k_1\Gamma^{x_3-1}\sqrt{P_0(P_0-P_1)}\cdot H_1\{(2P_1-P_0),\lambda\} \\
&+ k_1\Gamma^{x_3-1}\sqrt{P_0^2/2}\cdot(1-H_1\{(2P_1-P_0),\lambda\}) \\
N_2^H =& k_2(1-2(P_1-P_2)/3P_1)\cdot\sqrt{P_1(P_1-P_2)}H_1\{(2P_2-P_1),\lambda\} \\
&+ 0.471k_2P_1\cdot(1-H_1\{(2P_2-P_1),\lambda\}) \\
N_3^H =& k_3(1-2(P_2-P_3)/3P_2)\cdot\sqrt{P_2(P_2-P_3)}H_1\{(2P_3-P_2),\lambda\} \\
&+ 0.471k_3P_2\cdot(1-H_1\{(2P_3-P_2),\lambda\})
\end{aligned} \tag{26}$$

The distribution coefficients $H_1\left\{g\left(\boldsymbol{x},\boldsymbol{u}\right),\lambda\right\}$ and $\left(1-H_1\left\{g\left(\boldsymbol{x},\boldsymbol{u}\right),\lambda\right\}\right)$ function like switching mechanisms, dictating the activation of only one subsystem among the molar flow rate expressions N_1^H, N_2^H, and N_3^H at any given time. When H_1 is zero, $1-H_1$ becomes one, effectively toggling between the subsystems. This ensures that only one subsystem is operational while the others remain inactive. As a result, determining the the hybrid time trajectory T_τ and its accompanying hybrid mode trajectory T_μ becomes unnecessary for any specified $(\boldsymbol{\sigma},\boldsymbol{t})$.

Introducing the smoothed Heaviside function and using the integrated flow rate expressions, Problem 1 may be reformulated as Problem 2:

Problem 2

$$
\begin{aligned}
&\min_{\boldsymbol{\sigma},\boldsymbol{t}} J = t_F \\
s.t.& \\
&\dot{x_1} = \dot{P}_1 = \left(N_1^H - N_2^H\right)/V_{1e} \\
&\dot{x_2} = \dot{P}_2 = \left(N_2^H - N_3^H\right)/V_{2e} \\
&\dot{x_3} = \left(-x_3 + u_1\right)/\tau_m \\
&\forall t \in \left[t_{k-1}, t_k\right), k = 1, ..., N \\
&\boldsymbol{x}\left(t_0\right) = \boldsymbol{x}_0 \\
&\boldsymbol{x}\left(t_F\right) = \boldsymbol{x}_F \\
&G_1 = P_1 - \beta P_2 \leq 0
\end{aligned}
\tag{27}
$$

where the integrated molar flow rate expressions N_1^H, N_2^H, and N_3^H in Problem 2 refer to their definitions in (26). The formulated Problem 2 no longer requires determination of the corresponding hybrid time/mode trajectories T_τ/T_μ in advance for any given $(\boldsymbol{\sigma},\boldsymbol{t})$. Problem 2 is a regular OCP with state dynamic described by a continuous system. Notably the time horizon $[t_0, t_F]$ is partitioned into contiguous time stages $t \in [t_{k-1}, t_k)$ which allows the existence of one or several modes at each stage in Problem 2. In Problem 1, the time horizon is partitioned into contiguous epochs $I_q = [\tau_{q-1}, \tau_q)$ where only one mode can be active in each epoch. Note that use of the Heaviside approximation may result in a very stiff ODE

simulation, especially at switching times.

The LabVIEW interface allows piecewise constant input control policies only. This characteristic aligns with the foundation of CVP, where the control variables are parameterized. The variational method, also known as direct or trajectory sensitivity method will be employed to solve the proposed hybrid OCP Problem 2.

4.3 Sensitivity/Gradient Derivations

In the collocation method, the slack variables are used to transform inequality constraints into equality constraints.[27] Alternately, the CVP method typically uses Valentine's method[28,29] or penalty functions to handle inequality constraints. The presented work employs a smoothed penalty function approach as described in the work by Liu et al.[30] and Liu et al.[2]

When inequality constraints $G_j\left(\boldsymbol{x}\left(t\right),\boldsymbol{u}\left(t\right)\right)\leq 0, j=1,...,n_1$ are strictly satisfied, the integration of path violations should be zero.

$$\sum_{k=1}^{N}\int_{t_{k-1}}^{t_k}\max\left\{G_j\left(\boldsymbol{x}\left(t\right),\boldsymbol{u}\left(t\right)\right),0\right\}dt=0, j=1,...,n_1 \tag{28}$$

Here, n_1 is the total number of inequality constraints. The max function $\max\left\{G_j\left(\cdot\right),0\right\}$ denotes the choice of the greater between $G_j\left(\boldsymbol{x}\left(t\right),\boldsymbol{u}\left(t\right)\right)$ and 0. For readability, the two arguments $G_j\left(\boldsymbol{x}\left(t\right),\boldsymbol{u}\left(t\right)\right)$ and 0 in max function $\max\left\{\cdot\right\}$ and $G_j\left(\boldsymbol{x}\left(t\right),\boldsymbol{u}\left(t\right)\right)$ and the smoothing factor ϵ in the smoothed penalty function $spf\left\{\cdot\right\}$ in all following equations are enclosed in braces $\left\{\cdot\right\}$.

The optimization parameters are time-independent so the resulting Static Optimization Problem (SOP) in general Mayer form with max function is formulated as SOP_1 with corresponding objective function J_1:

SOP_1

$$\min_{\boldsymbol{\sigma},\boldsymbol{t}} J_1 = \Phi_0\left(\boldsymbol{x}\left(t_F|\boldsymbol{\sigma},\boldsymbol{t}\right)\right) + \sum_{k=1}^{N}\int_{t_{k-1}}^{t_k} L_0\left(\boldsymbol{x}\left(t|\boldsymbol{\sigma},\boldsymbol{t}\right),\boldsymbol{u}\left(t|\boldsymbol{\sigma},\boldsymbol{t}\right),t\right)dt$$

$$s.t.\sum_{k=1}^{N}\int_{t_{k-1}}^{t_k}\max\left\{G_j\left(\boldsymbol{x}\left(t|\boldsymbol{\sigma},\boldsymbol{t}\right),\boldsymbol{u}\left(t|\boldsymbol{\sigma},\boldsymbol{t}\right)\right),0\right\}dt = 0, j = 1,...,n_1 \tag{29}$$

The max function $\max\{G_j, 0\}$ is non-negative regardless of whether the constraints $G_j \leq 0$ are satisfied or not. Consequently the max function can be added to original objective J_1 by multiplying with a weighting parameter ρ, resulting in a new objective function J_2 corresponding to SOP_2 with no path constraints.

SOP_2

$$\min_{\boldsymbol{\sigma},\boldsymbol{t}} J_2 = J_1 + \rho\cdot\sum_{k=1}^{N}\int_{t_{k-1}}^{t_k}\sum_{j=1}^{n_i}\max\left\{G_j\left(\boldsymbol{x}\left(t|\boldsymbol{\sigma},\boldsymbol{t}\right),\boldsymbol{u}\left(t|\boldsymbol{\sigma},\boldsymbol{t}\right)\right),0\right\}dt \tag{30}$$

Some concerns related to application of the penalty function with (28) for OCP solving were presented by Barton:[14] The max function $\max\{G_j, 0\}$ is continuous but non-smooth. Accordingly, the SOP_2 is inherently a discrete OCP and first order gradient information can not be obtained within the framework of CVP. Additionally, numerical difficulties may arise because this formulation requires $\rho \to \infty$ to exactly satisfy the constraint precisely. A smoothed penalty function approach is employed to approximate the max function in J_2 so that the gradient information can be computed within an acceptable error tolerance. The idea was proposed first by Bryson[31] and a detailed algorithm was later presented by Liu et al.[30] A smoothed function which approximates $\max\{G_j, 0\}$ is given as:[2,30]

$$spf\left\{G_j,\epsilon\right\} = \frac{1}{2}\left(G_j\left(\boldsymbol{x}\left(t\right),\boldsymbol{u}\left(t\right)\right) + \sqrt{G_j^2\left(\boldsymbol{x}\left(t\right),\boldsymbol{u}\left(t\right)\right) + 4\epsilon^2}\right) \tag{31}$$

where ϵ is the smoothing factor, $\epsilon > 0$. By substituting the smoothed function $spf\{G_j, \epsilon\}$ for max function $\max\{G_j, 0\}$ in eq 30, the new objective function J_3 is written as follows corresponding to SOP_3:

SOP_3

$$\min_{\boldsymbol{\sigma},\boldsymbol{t}} J_3 = J_1 + \rho \cdot \sum_{k=1}^{N} \int_{t_{k-1}}^{t_k} \sum_{j=1}^{n_1} spf\left\{G_j\left(\boldsymbol{x}\left(t|\boldsymbol{\sigma},\boldsymbol{t}\right),\boldsymbol{u}\left(t|\boldsymbol{\sigma},\boldsymbol{t}\right)\right),\epsilon\right\} dt \tag{32}$$

where the smoothed penalty function spf is defined in (31).

The objective J_3 is continuous and smooth, assuming G_j is continuous and smooth. Then the first order gradient information can be evaluated using the trajectory sensitivity method. Furthermore, an iterative algorithm Algorithm 1 is proposed to obtain more accurate optimal controls by gradually increasing the penalty factor ρ and decreasing smoothing factor ϵ.[30] Corresponding to smoothed penalty function $spf\left\{G_j\left(\cdot\right),\epsilon\right\}$, the updating formula for smoothing factor ϵ in k_p^{th} iteration is presented as:[30]

$$\epsilon^{(k_p)} = 2\varsigma / \left(\left(1+\sqrt{5}\right)\rho^{(k_p)} n_1 \left(t_F - t_0\right)\right) \tag{33}$$

Error analysis proves[30] that if the smoothing factor ϵ is sufficiently small, the solution of SOP_3 is approximately the solution to SOP_1. The proof showing the error between solutions to SOP_1 and SOP_3 within minimal tolerance is also available[30]. Consequently the implementation of Algorithm 1 does not necessarily require $\rho \to \infty$ to obtain an exactly solution to SOP_1 thus no numerical difficulty is expected. The form of the penalty function is not unique, and an alternative penalty function in the form of a piecewise function is feasible.[32] In prior research,[33] the penalty function defined in (31) was adopted, and its precision was validated through case studies to align with the results achieved by the popular optimization package Pyomo[34] and the Ipopt solver. Therefore, this study maintains the use of the penalty function specified in (31).

When incorporating the variable switching times $\boldsymbol{t}$ as decision variables, the discontinuity in sensitivity values at the switching times $\boldsymbol{t}$ cannot be dismissed. This discontinuity is

Algorithm 1 Iterative algorithm for the smoothed penalty function approach

Step 1. Set up the iteration number $k_p = 1$, initial penalty factor $\rho^{(k_p)}$, initial smoothing factor $\epsilon^{(k_p)}$, and tolerance ς.
Step 2. Input the initial decision variable vector $\boldsymbol{z}^{(k_p)} = (\boldsymbol{\sigma}, \boldsymbol{t})$.
Step 3. Solve the OCP with trajectory sensitivity approach, obtain new decision variable vector $\boldsymbol{z}^{(k_p+1)}$.
Step 4. Decide whether the decision variable vector converge by $\left|J_3\left(\boldsymbol{z}^{(k_p+1)}\right) - J_3\left(\boldsymbol{z}^{(k_p)}\right)\right| \leq \varsigma$.
If satisfied, output $\boldsymbol{z}^{(k_p+1)}$ as an approximate solution.
If not satisfied, continue to Step 5.
Step 5. Increment the iteration index $k_p = k_p + 1$, $\boldsymbol{z}^{(k_p)} = \boldsymbol{z}^{(k_p+1)}$. Update $\rho^{(k_p+1)} = c^{(k_p)}\rho^{(k_p)}$ and $\epsilon^{(k_p+1)} = d^{(k_p)}\epsilon^{(k_p)}$, $c^{(k_p)}d^{(k_p)} = 1\,(c > 1, 0 < d < 1)$. Go back to Step 2.

typically described by the transfer function, which is also known as the jump condition.[14,35,36] When the switching times are variable, it may be cumbersome to integrate the state and sensitivity systems numerically.[37] Loxton and Teo et al. proposed a Control Parameterization Enhance Transform (CPET) technique to overcome this difficulty by mapping the time scale to a new time scale.[1,38,39] If the length of each time stage δ_k is flexible, a normalized time variable s is introduced by time scaling transformation of Loxton as:[40]

$$\begin{aligned} dt &= \delta_k ds = \delta_{\lfloor s \rfloor + 1} ds, \\ k &= 1, .., N \end{aligned} \tag{34}$$

where $\lfloor s \rfloor$ is the floor function of s. The relation of $t\,(s)$ from $t \in [t_{k-1}, t_k)$ to the new time scale $s \in [k-1, k)$ is given as:

$$t\,(s) = [s - (k-1)]\,(t_k - t_{k-1}) + t_{k-1} \tag{35}$$

New state variables $\bar{\boldsymbol{x}}$, control variables $\bar{\boldsymbol{u}}$, and vector function $\bar{\boldsymbol{f}}$ are defined in the s domain. Additionally, the new objective function, equality constraints, and inequality constraints are included in vector form $\bar{\boldsymbol{G}}$, where the values are equivalent to their originals:

$$\bar{\boldsymbol{x}}(s) = \boldsymbol{x}(t) = \boldsymbol{x}(t(s))$$

$$\bar{\boldsymbol{u}}(s) = \boldsymbol{u}(t(s))$$

$$\bar{\boldsymbol{f}}(\bar{\boldsymbol{x}}(s), \bar{\boldsymbol{u}}(s)) = \boldsymbol{f}(\boldsymbol{x}(t), \boldsymbol{u}(t)) = \boldsymbol{f}(\bar{\boldsymbol{x}}(s), \bar{\boldsymbol{u}}(s))$$

$$\bar{\boldsymbol{G}}(\bar{\boldsymbol{x}}(s), \bar{\boldsymbol{u}}(s)) = \boldsymbol{G}(\boldsymbol{x}(t), \boldsymbol{u}(t)) = \boldsymbol{G}(\bar{\boldsymbol{x}}(s), \bar{\boldsymbol{u}}(s)) \tag{36}$$

As a result, the state equation ODE after the time scaling is obtained as:

$$\dot{\bar{\boldsymbol{x}}}(s) = \delta_k \boldsymbol{f}(\bar{\boldsymbol{x}}(s|\boldsymbol{\sigma}, \boldsymbol{\delta}), \bar{\boldsymbol{u}}(s|\boldsymbol{\sigma}, \boldsymbol{\delta})),$$
$$\forall s \in [k-1, k), k = 1, ..., N \tag{37}$$

In the time-scaled problem, the class of decision variables that need to be solved for has shifted from the switching times $\boldsymbol{t}$ in Problem 3 to the lengths of time intervals $\boldsymbol{\delta}$, although $\boldsymbol{t}$ and $\boldsymbol{\delta}$ are intrinsically the same type of decision variables, determining $\boldsymbol{t}$ inherently dictates $\boldsymbol{\delta}$.

By adopting the CPET technique to transform Problem 2 to mitigate sensitivity discontinuity, the resulting optimization problem can be denoted as Problem 3. For readability, the bar symbol indicating time-scaling has been omitted from the letters. The time scale can be discerned by examining the time variable inside the parenthesis: $\boldsymbol{x}(t|\boldsymbol{\sigma}, \boldsymbol{t})$ or $\boldsymbol{x}(s|\boldsymbol{\sigma}, \boldsymbol{\delta})$.

Problem 3

$$
\begin{aligned}
&\min_{\boldsymbol{\sigma},\boldsymbol{\delta}} J = \sum_{k=1}^{N} \delta_k + \rho \cdot x_4\left(N\right) \\
s.t.& \\
&\dot{x_1} = \dot{P}_1 = \delta_k \left(N_1^H - N_2^H\right)/V_{1e} \\
&\dot{x_2} = \dot{P}_2 = \delta_k \left(N_2^H - N_3^H\right)/V_{2e} \\
&\dot{x_3} = \delta_k \left(-x_3 + u_1\right)/\tau_m \\
&\dot{x_4} = \delta_k \left(\left(P_1 - \beta P_2\right) + \sqrt{\left(P_1 - \beta P_2\right)^2 + 4\epsilon^2}\right)/2 \\
&\forall s \in \left[k-1, k\right), k = 1, ..., N \\
&\boldsymbol{x}\left(0\right) = \boldsymbol{x}_0 \\
&\boldsymbol{x}\left(N\right) = \boldsymbol{x}_F
\end{aligned} \tag{38}
$$

where an additional variable x_4 has been incorporated to account for the integration of path violation of G_1. This modification transforms the Lagrange term of eq 32 into a Mayer term x_4 facilitating problem solution.

The OCP formatted by Problem 3 is subsequently solved using the sensitivity method. The sensitivity coefficients $\boldsymbol{\phi}_{i,k}$ and $\boldsymbol{\psi}_k$ are partial derivatives of the state variables from eq 37 with respect to the control values $\sigma_{i,k}$ and time interval lengths δ_k in the transformed time domain, respectively:

$$
\boldsymbol{\phi}_{i,k}\left(s\right) = \frac{\partial \boldsymbol{x}\left(s|\boldsymbol{\sigma},\boldsymbol{\delta}\right)}{\partial \sigma_{i,k}}, i = 1, ..., n_u, k = 1, ..., N \tag{39}
$$

$$
\boldsymbol{\psi}_k\left(s\right) = \frac{\partial \boldsymbol{x}\left(s|\boldsymbol{\sigma},\boldsymbol{\delta}\right)}{\partial \delta_k}, k = 1, ..., N \tag{40}
$$

Note $\boldsymbol{\phi}_{i,k}\left(s\right) \in \mathbb{R}^{n_x}$ and $\boldsymbol{\psi}_k\left(s\right) \in \mathbb{R}^{n_x}$. In Problem 3 the integration of path violations is represented by the variable x_4. Therefore, for Problem 3, the dimension of state variables for Problem 3, denoted as n_x, is calculated as $n_x = 3 + 1 = 4$.

The corresponding sensitivity equations may be derived by taking the partial derivative of eq 37 with respect to $\sigma_{i,k}$ and δ_k in transformed time domain s:

$$\dot{\boldsymbol{\phi}}_{i,k}(s) = \sum_{l=k}^{N} \delta_l \frac{\partial \boldsymbol{f}\left(\boldsymbol{x}\left(s|\boldsymbol{\sigma},\boldsymbol{\delta}\right),\boldsymbol{u}\left(s|\boldsymbol{\sigma},\boldsymbol{\delta}\right)\right)}{\partial \boldsymbol{x}} \boldsymbol{\phi}_{i,k}(s)\, \chi_{[l-1,l)}(s) + \delta_k \frac{\partial \boldsymbol{f}\left(\boldsymbol{x}\left(s|\boldsymbol{\sigma},\boldsymbol{\delta}\right),\boldsymbol{u}\left(s|\boldsymbol{\sigma},\boldsymbol{\delta}\right)\right)}{\partial u_i} \chi_{[k-1,k)}(s) \tag{41}$$

$$\dot{\boldsymbol{\psi}}_{k}(s) = \sum_{l=k}^{N} \delta_l \frac{\partial \boldsymbol{f}\left(\boldsymbol{x}\left(s|\boldsymbol{\sigma},\boldsymbol{\delta}\right),\boldsymbol{u}\left(s|\boldsymbol{\sigma},\boldsymbol{\delta}\right)\right)}{\partial \boldsymbol{x}} \boldsymbol{\psi}_{k}(s)\, \chi_{[l-1,l)}(s) + \boldsymbol{f}\left(\boldsymbol{x}\left(s|\boldsymbol{\sigma},\boldsymbol{\delta}\right),\boldsymbol{u}\left(s|\boldsymbol{\sigma},\boldsymbol{\delta}\right)\right) \chi_{[k-1,k)}(s) \tag{42}$$

The final functions for the computation of first-order gradient in s time scale/domain are given as:[33]

$$\frac{\partial G_j}{\partial \sigma_{i,k}} = \frac{\partial \Phi_j\left(\boldsymbol{x}\left(N|\boldsymbol{\sigma},\boldsymbol{\delta}\right)\right)}{\partial \boldsymbol{x}} \boldsymbol{\phi}_{i,k}(N) + \sum_{l=k}^{N} \int_{l-1}^{l} \delta_l \frac{\partial L_j\left(\boldsymbol{x}\left(s|\boldsymbol{\sigma},\boldsymbol{\delta}\right),\boldsymbol{u}\left(s|\boldsymbol{\sigma},\boldsymbol{\delta}\right)\right)}{\partial \boldsymbol{x}} \boldsymbol{\phi}_{i,k}(s)\, ds + \int_{k-1}^{k} \delta_k \frac{\partial L_j\left(\boldsymbol{x}\left(s|\boldsymbol{\sigma},\boldsymbol{\delta}\right),\boldsymbol{u}\left(s|\boldsymbol{\sigma},\boldsymbol{\delta}\right)\right)}{\partial u_i} ds \tag{43}$$

$$\frac{\partial G_j}{\partial \delta_k} = \frac{\partial \Phi_j\left(\boldsymbol{x}\left(N|\boldsymbol{\sigma},\boldsymbol{\delta}\right)\right)}{\partial \boldsymbol{x}} \boldsymbol{\psi}_{k}(N) + \sum_{l=k}^{N} \int_{l-1}^{l} \delta_l \frac{\partial L_j\left(\boldsymbol{x}\left(s|\boldsymbol{\sigma},\boldsymbol{\delta}\right),\boldsymbol{u}\left(s|\boldsymbol{\sigma},\boldsymbol{\delta}\right)\right)}{\partial \boldsymbol{x}} \boldsymbol{\psi}_{k}(s)\, ds + \int_{k-1}^{k} L_j\left(\boldsymbol{x}\left(s|\boldsymbol{\sigma},\boldsymbol{\delta}\right),\boldsymbol{u}\left(s|\boldsymbol{\sigma},\boldsymbol{\delta}\right)\right) ds \tag{44}$$

In the following section, the derived sensitivity formulas from (41) and (42) and the gradient formulas from (43) and (44) are employed. When combined with specific experimental settings, the open-loop optimization problem corresponding to Problem 3 can be solved. Note that the experimental system momentarily exceeds the constraint $P_2 \leq 1.5P_1$. This shows that a safety margin should be incorporated into any system when the slightest excursion into an unsafe mode can not be tolerated.

5 Results and Discussion

The implementation was carried out using MATLAB version 2023a. The optimization process involved the use of the ODE solver 'ode45' and the NLP solver 'fmincon'. In order to achieve accurate optimization outcomes for Problem 3, the tolerances of the ODE solver tolerances were configured as AbsTol = RelTol = 10^{-8}. Accordingly, the NLP solver tolerances were set to TolX = TolFun = TolCon = 10^{-6}.The parameter λ governing the behavior of the smoothed Heaviside function H_1 was established at $\lambda = 10^4$. The Sequential Quadratic Programming (SQP) algorithm was employed, with Algorithm 1 parameters initialized as $c = 10$, $d = 0.1$, $\varsigma = 2 \times 10^{-4}$, and $\rho^{(1)} = 1$.

The feed pressure P_0 was set to be constant at 75.00 psia. The atmospheric pressure P_3 was specified as 14.67 psia. Both of these pressures are held constant throughout the optimization simulation. Initially, both Tank 1 and Tank 2 have pressures close to the atmospheric value, specifically given by $\boldsymbol{x}_0 = (14.69, 14.68)$ psia. Given an acceptable control input, it is anticipated that the system will achieve the terminal state of $x_F = (73.77, 56.67)$ psia. This terminal state corresponds to a steady state where $u_1 = 75\%$. The goal of the optimization is to arrive at this terminal state $\boldsymbol{x}_F$ in the shortest possible time while adhering to specific state constraints. This simulation essentially mirrors the start-up process of a plant, with a selected valve V_{12} satisfying an illustrative constraints $G_1 = P_1 - 1.5P_2$ as explained in the previous section.

Table 3 presents the parameter values of the optimization process and the optimal objectives for each iteration as determined by Algorithm 1. Figure 8 illustrates the optimal state trajectories, while Figure 9 displays them in the phase plane. The optimal decision variables are outlined in Table 4, where $\sigma_{1,k}$ denotes the control heights of CV_1 and δ_k denotes the lengths of the time intervals.

Table 3: Penalty process for Problem 3

Iteration	Penalty factor ρ	Smoothing factor ϵ	$x_4\,(s=N)$	$J^*_{3,\min}$
1	10^0	1.2361×10^{-4}	0.0952	40.5672
2	10^1	1.2361×10^{-5}	8.7874×10^{-5}	40.6116
3	10^2	1.2361×10^{-6}	1.3971×10^{-7}	40.6122
4	10^3	1.2361×10^{-7}	1.1809×10^{-10}	40.6120

Table 4: Optimal control policy for Problem 3

k^{th} Stage	1	2	3	4	5	6
$\sigma_{1,k}$	38.94	46.44	55.45	67.96	100.00	0.00
δ_k	14.54	4.98	4.57	3.93	11.80	0.79

CPU Time: 31.918 s

6 Conclusions

A high-fidelity autonomous hybrid model developed from experimental data was presented. This model describes the hybrid dynamic process of air flow in a tank system with choked flow phenomenon taken into consideration. The developed hybrid dynamic model was used for solution of optimal control problems. The goal was to minimize the transition time from one steady state to another without violation of specified path constraints. The path constraints originate from forcing the system to avoid extreme choked flow during the transition. Determination of the mode and time sequence of the hybrid dynamic system when applying sensitivity to both parameter estimation and OCP was avoided by introducing a smoothed Heaviside function. In order to protect specific valves against excessive choked flow, the application of Problem 3 could be expanded to more harsh work situations with higher feed pressure P_0. Other binary piecewise systems could benefit from the implementation of smoothed Heaviside function.

The application of the smoothed Heaviside function excels in seamlessly transitioning

between two subsystems. However, when the number of subsystems surpasses two, a re-evaluation of this approach may be needed. In the context of the system considered in this work, the gas supply pressure consistently exceeds the downstream pipeline so a unidirectional flow is considered. Given a valve designed for bidirectional flow accommodating both forward and reverse directions, it becomes essential to include an additional representation to precisely illustrate the four distinct scenarios arising from combinations of forward/reverse flow and normal/choked flow conditions. In such scenarios, introducing multi-dimensional smoothing functions or a combination of multiple smoothed Heaviside functions could be more appropriate. In practical applications, especially with frequent valve state alterations, capturing these four distinct flow states accurately can be challenging. Each flow state transition might come with its own set of conditions, complicating control strategies. Moreover, integrating these four flow states could introduce added uncertainties and potential instability to the system. This necessitates meticulous considerations during control strategy designs. In conclusion, while the smoothed Heaviside function proves commendable in binary systems, its stability and performance might require further scrutiny and adjustments in more intricate scenarios.

Another direction for further investigation involves the parameter λ in the smoothed Heaviside function used in current study. This parameter λ adjusts the steepness of the smooth approximation. Currently, the parameter λ used in the smoothed Heaviside function determining the steepness was predetermined. Future work may focus on investigating the relationship between the chosen value of λ and the introduced approximation error when compared to the regular Heaviside function. It is essential to note that the approximation error due to smoothing is dependent on the value of λ. Consequently, it is imperative to ensure that such an approximation neither compromises the stability of the system nor diminishes its performance and that the value of λ is adjusted according to the specific application needs.

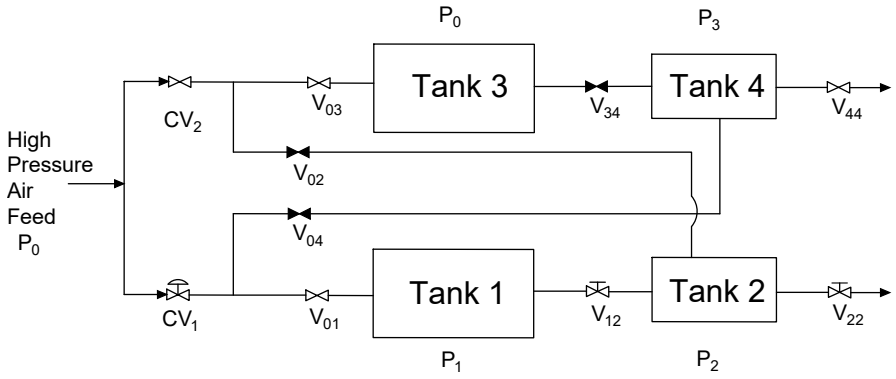

Figure 1: Flowsheet of experimental tank apparatus in the two-tanks in series format. Note this arrangement allows the pressure of tank 3 to mirror the feed pressure P_0 and the pressure of tank 4 matching the atmospheric pressure P_3.

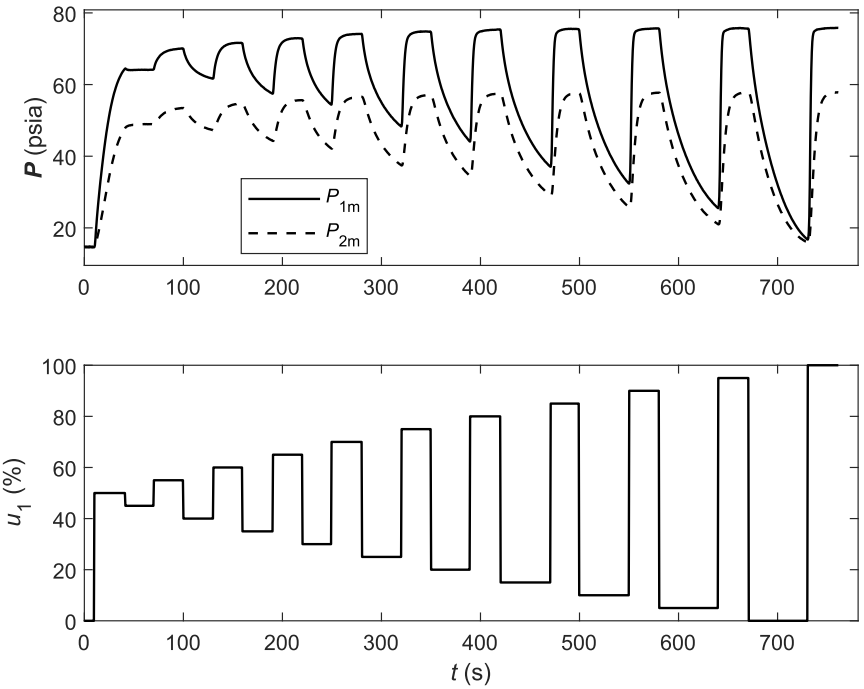

Figure 2: Experimental data $P_{1\mathrm{m}}$ and $P_{2\mathrm{m}}$ for specified control policy.

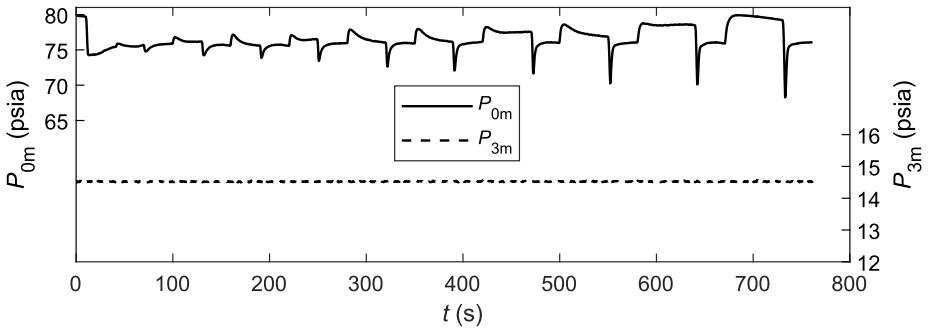

Figure 3: Experiment data of $P_{0\mathrm{m}}$ and $P_{3\mathrm{m}}$ versus time.

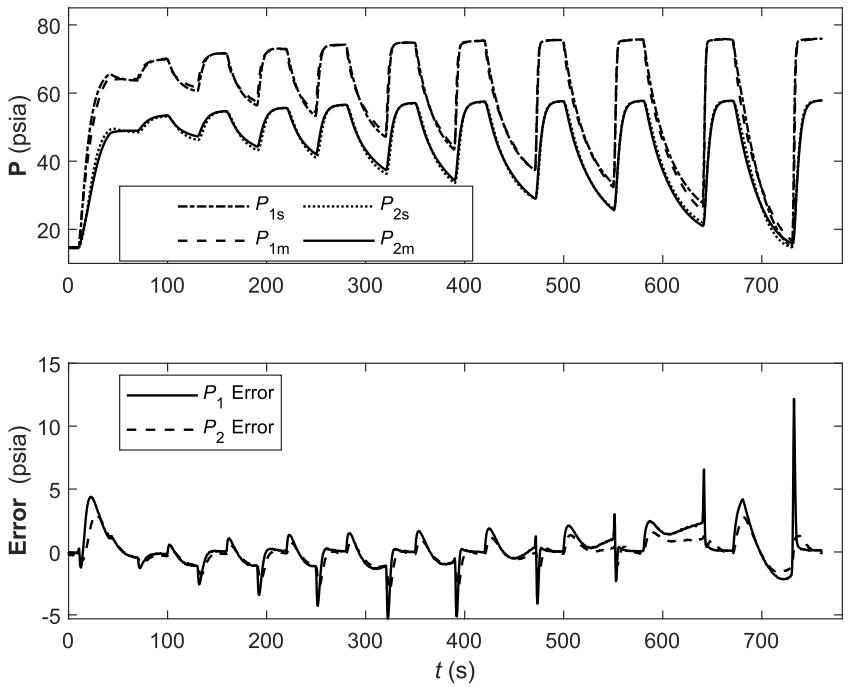

Figure 4: Simulated states $P_{1\mathrm{s}}$ and $P_{2\mathrm{s}}$ versus measured states $P_{1\mathrm{m}}$ and $P_{2\mathrm{m}}$ (top) and simulated/measured error (bottom).

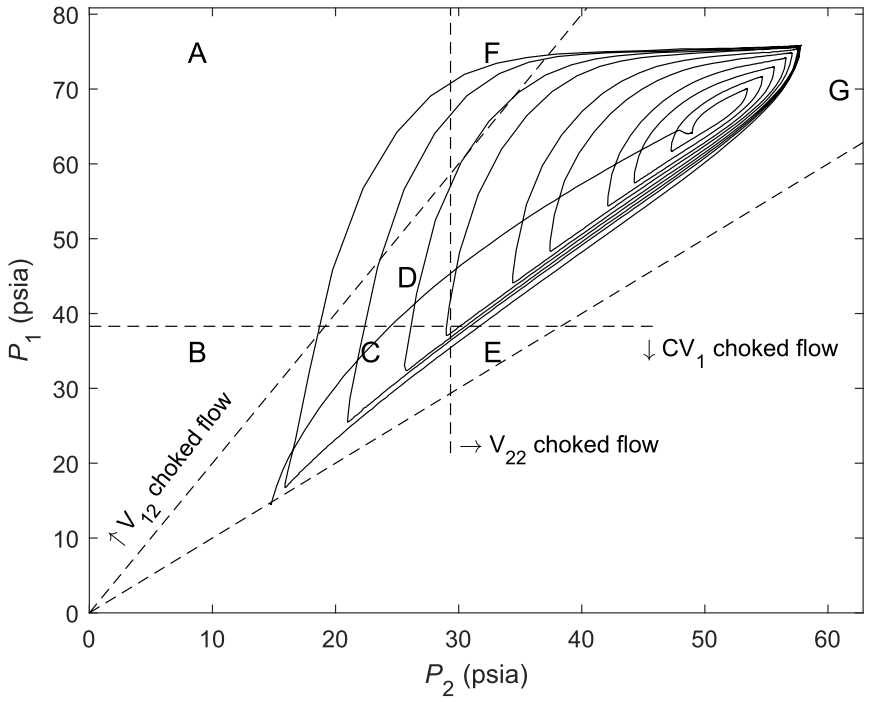

Figure 5: Phase plane plot of experimental pressure data $P_{1\mathrm{m}}$ and $P_{2\mathrm{m}}$ versus time. Note for some regions such as region A and B, the common boundaries are line segments, while for others such as region A and C, the common boundaries consist only of a point.

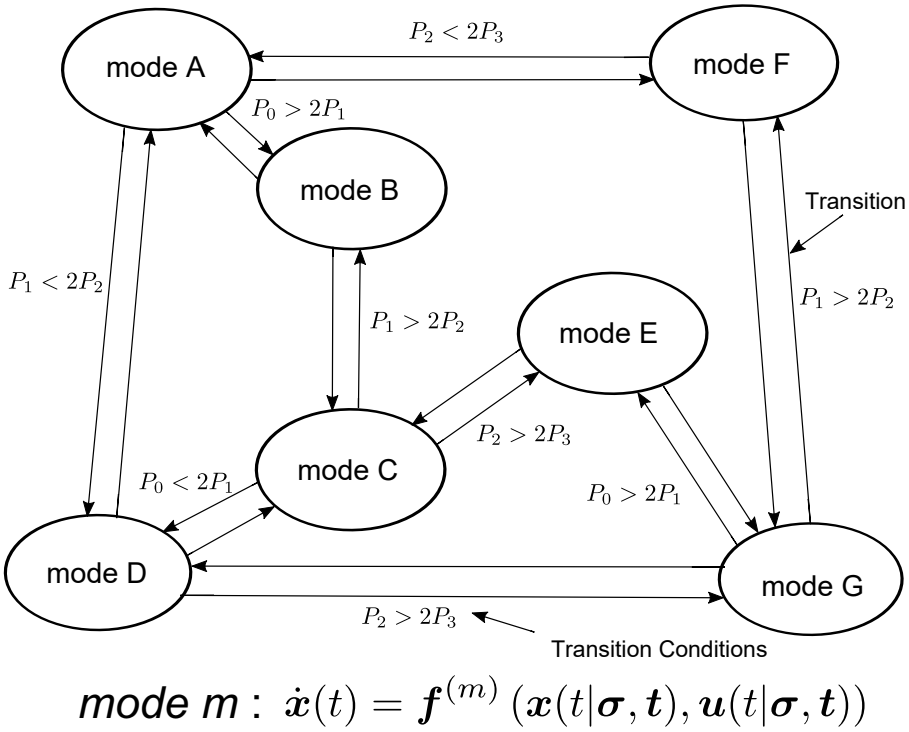

Figure 6: Continuous time hybrid automaton of the illustrated hybrid system due to choked flow. Note if the common boundary between mode regions in phase plane Figure 5 is merely a point, the transition between these modes is not depicted in this automaton diagram.

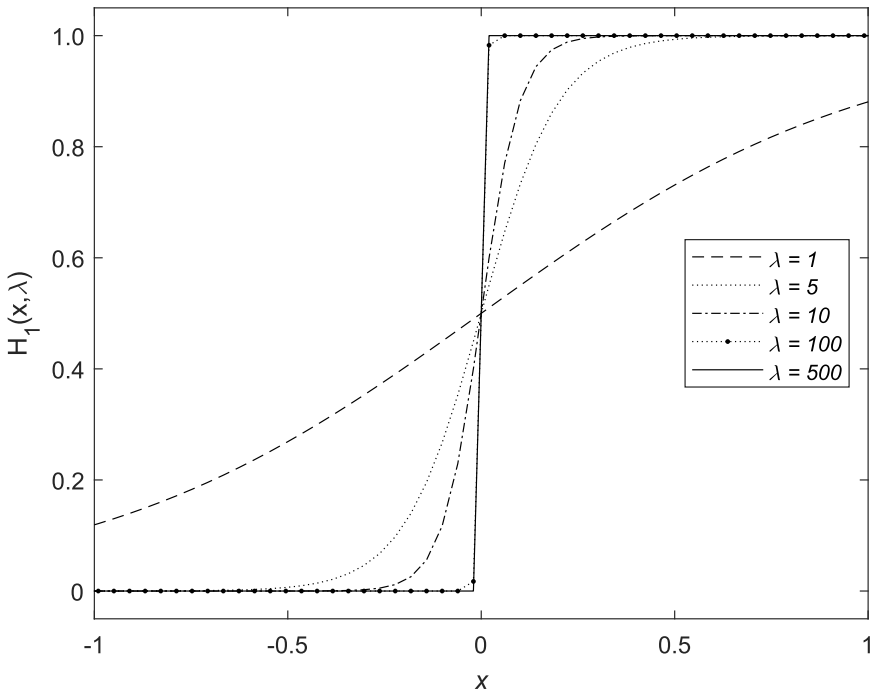

Figure 7: Smoothed Heaviside functions $H_1(x, \lambda)$ with different λ values.

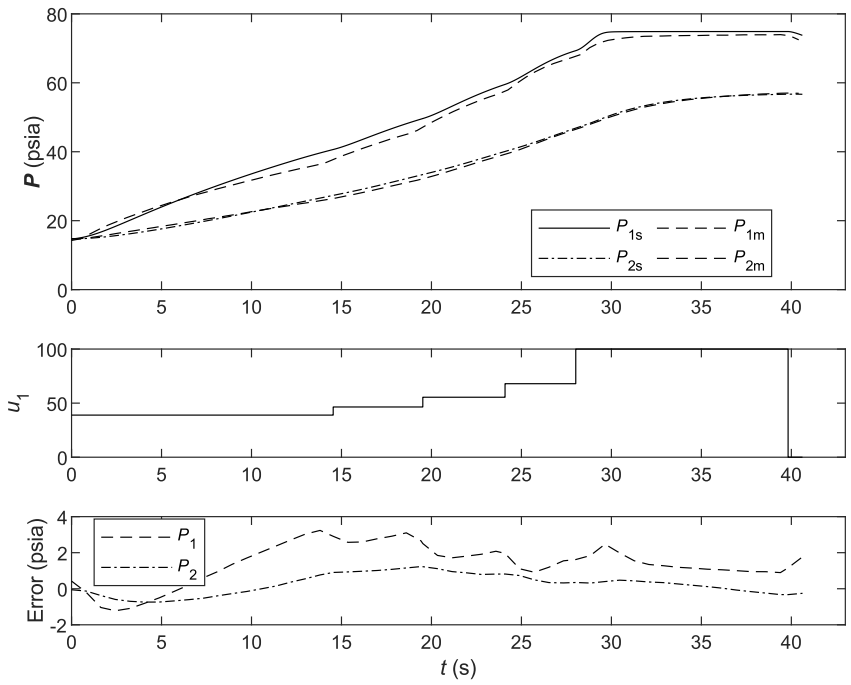

Figure 8: Experimental states $P_{1\mathrm{m}}$ and $P_{2\mathrm{m}}$ versus simulated states $P_{1\mathrm{s}}$ and $P_{2\mathrm{s}}$ with predicted control policy.

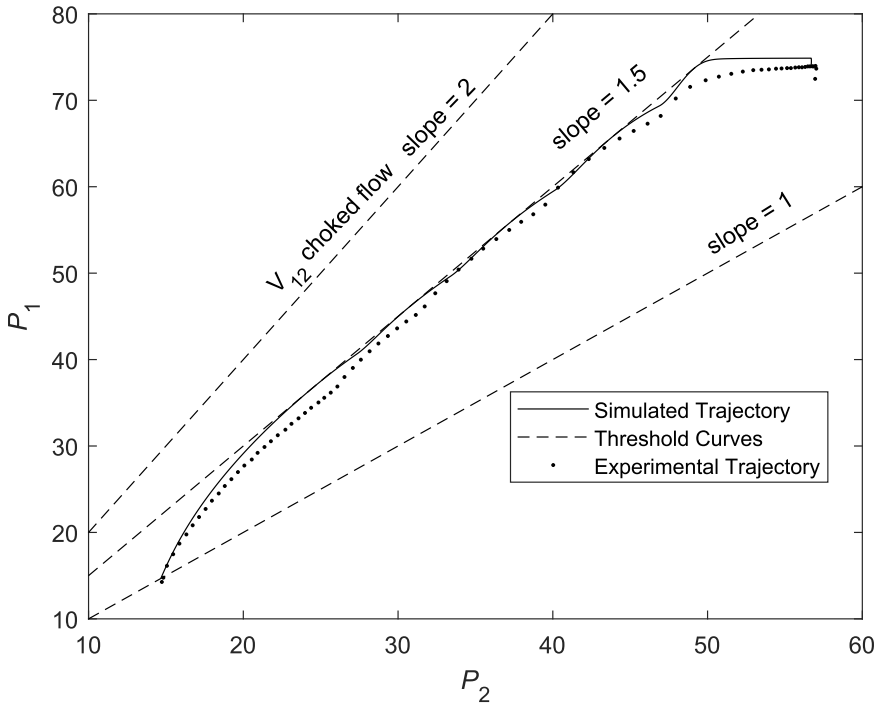

Figure 9: Phase plane plot of $P_{1\mathrm{m}}$ and $P_{2\mathrm{m}}$ versus time with predicted control policy.

References

[1] K. L. Teo, B. Li, C. Yu, and V. Rehbock. Applied and computational optimal control. *Optimization and Its Applications*, 2021.

[2] Hang Liu, Ping Liu, Xinggao Liu, and Hailong Huang. Adaptive control arc length-based time grid refinement control parameterisation method for unmanned hypersonic vehicle reentry trajectory optimisation. *International Journal of Control*, 96(10):2565–2575, 2023.

[3] P. I. Barton, C. K. Lee, and M. Yunt. Optimization of Hybrid Systems. *Computers Chem. Engineering*, 30:1576–1589, 2006.

[4] W.P.M.H. Heemels, B. De Schutter, and A. Bemporad. Equivalence of hybrid dynamical models. *Automatica*, 37(7):1085–1091, 2001.

[5] Gianluca Serale, Massimo Fiorentini, Alfonso Capozzoli, Daniele Bernardini, and Alberto Bemporad. Model predictive control (mpc) for enhancing building and hvac system energy efficiency: Problem formulation, applications and opportunities. *Energies*, 11(3):631, 2018.

[6] Weifeng Zhong, Qun Lin, Ryan Loxton, and Kok Lay Teo. Optimal train control via switched system dynamic optimization. *Optimization Methods and Software*, 36(2-3):602–626, 2021.

[7] Chongyang Liu, Zhaohua Gong, Kok Lay Teo, Jie Sun, and Louis Caccetta. Robust multi-objective optimal switching control arising in 1, 3-propanediol microbial fed-batch process. *Nonlinear Analysis: Hybrid Systems*, 25:1–20, 2017.

[8] P. I. Barton and C. C. Pantelides. Modeling of combined discrete/continuous processes. *Process Systems Engineering*, 40:966–979, 1994.

[9] A. Bemporad and M. Morari. Control of Systems Integrating Logic, Dynamics, and Constraints. *Automatica*, 35:407–427, 1999.

[10] R. A. DeCarlo, M. S. Branicky, S. Pettersson, and B. Lennartson. Perspectives and Results on the Stability and Stabilitzability of Hybrid Systems. *Proceedings of the IEEE*, 88:1069–1082, 2000.

[11] R. Alur, C. Courcoubetis, T. A. Henzinger, and P. H. Ho. Hybrid Automata: An Algorithmic Approach to the Specification and Verification of Hybrid Systems, 1992.

[12] R. Alur, C.Courcoubetis, N. Halbwachs, T. A. Henzinger, P. H. Ho, X. Nicollin, A. Olivero, J. Sifakis, and S. Yovine. The Algorithmic Analysis of Hybrid System. *Theoretical Computer Science*, 138:3–34, 1995.

[13] V. D. Dimitriadis, N. Shah, and C. C. Pantelides. Modeling and Safety Verification of Discrete/Continuous Processing Systems. *AICHE Journal*, 43:1041–1059, 1997.

[14] W. F. Feehery and P. I. Barton. Dynamic optimization with state variable path constraints. *Computers and Chemical Engineering*, 22:1241–1256, 1998.

[15] P. I. Barton, J. R. Banga, and S. Gala. Optimization of Hybrid Discrete/Continuous Dynamic Systems. *Computers Chem. Engineering*, 24:2171–2182, 2000.

[16] P. I. Barton and C. K. Lee. Modeling, Simulation and Sensitivity Analysis of Hybrid Systems. *IEEE International Symposium on Computer-Aided Control System Design*, 2002.

[17] S. Galan, W. F. Feehery, and P. I. Barton. Parametric Sensitivity Functions for Hybrid Discrete/Continuous Systems. *Applied Numerical Mathematics*, 31:17–47, 1999.

[18] P. I. Barton, C. K. Lee, and M. Yunt. Design of Process Operations using Hybrid Dynamic Optimization. *Computers Chem. Engineering*, 28:955–969, 2004.

[19] C.E. Long, J.D. Miles, C.E. Holland, and E.P. Gatzke. A flexible multivariable experimental air tank system for process control education. In *Proceedings of the 2003 American Control Conference, 2003.*, volume 1, pages 688–693 vol.1, 2003.

[20] Roy S Baty and Len G Margolin. Modern infinitesimals and the entropy jump across an inviscid shock wave. *International Journal of Aeroacoustics*, 17(4-5):502–520, 2018.

[21] F. Assassa and M. Marquardt. Optimality-based grid adaptation for input-affine optimal control problems. *Computers and Chemical Engineering*, 92:189–203, 2016.

[22] Don W Green and Robert H Perry. *Perry's chemical engineers' handbook*. McGraw-Hill Education, 2008.

[23] P. I. Barton, C. K. Lee, and M. Yunt. Optimization of Hybrid Systems. *Computers Chem. Engineering*, 30:1576–1589, 2006.

[24] BadgerMeter, Inc.: Industrial Division, Tulsa, OK. *Research Control Valves: Installation, Operation, and Maintenance Procedures*.

[25] Swagelok Company. *Swagelok: Valve Sizing*, August 2000.

[26] J. J. Casares and J. Rodriguez. Analysis and evaluation of a wastewater treatment plant model by stochastic optimization. *Applied Mathematical Modelling*, 13(7):420–424, 1989.

[27] J. Nocedal and S. J. Wright. *Numerical optimization*. Springer, 2006.

[28] D. H. Jacobson and M. M. Lele. A transformation technique for optimal control problems with a state variable in inequality constraint. *IEEE Transactions on Automatic Control*, 5:457–464, 1969.

[29] D. H. Jacobson and M. M. Lele. New necessary conditions of optimality for control problems with state variable inequality constraints. *Journal of Mathematical Analysis and Applications*, 35:255–284, 1971.

[30] X. Liu, Y. Hu, J. Feng, and K. Liu. A novel penalty approach for nonlinear dynamic optimization problems with inequality path constraints. *IEEE Transactions on Automatic Control*, 59(10):2863–2867, 2014.

[31] A. E. Bryson and Y. Ho. *Applied Optimal Control*. Taylor and Francis, Hemisphere, New York, 1975.

[32] P. Liu, X. Li, X. Liu, and Y. Hu. An improved smoothing technique-based control vector parameterization method for optimal control problems with inequality path constraints. *Optimal Control Applications and Methods*, 38:586–600, 2017.

[33] Hainan Wang, Xinhong Liu, and Edward P Gatzke. Time scaling transformation avoiding sensitivity discontinuity for nonlinear optimal control. *Industrial & Engineering Chemistry Research*, 62(36):14407–14426, 2023.

[34] M. B. Bynum, G. A. Hackeheil, W. E. Hart, C. D. Laird, B. L. Nicholson, J. D. Siirola, J. Watson, and D. L. Woodruff. *Pyomo-Optimization Modeling in Python*. Springer International Publishing, Hemisphere, New York, 2021.

[35] O. Rosen and R. Luus. Evaluation of gradients for piecewise constant optimal control. *Computers and Chemical Engineering*, 15:273–281, 1991.

[36] T. Hirmajer, E. B. Canto, and J. R. Banga. DOTcvpSB:a Matlab Toolbox for dynamic optimization in systems biology. Technical report, Instituto de Investigacions Marinas, IIM-CSIC, 2010.

[37] Q. Lin, R. Loxton, and K. L. Teo. The control parameterization method for nonlinear optimal control: a survey. *Journal of Industrial and management optimization*, 10(1):275–309, 2014.

[38] R. C. Loxton, K. L. Teo, and V. Rehbock. Optimal control problems with multiple

characteristic time points in the objective and constraints. *Automatica*, 44(11):2923–2929, 2008.

[39] R. Loxton, Q. Lin, and K. L. Teo. Switching time optimization for nonlinear switched systems: direct optimization and the time-scaling transformation. *Pacific Journal of Optimization*, 10(3):537–560, 2014.

[40] R. C. Loxton, K. L. Teo, and V. Rehbock. Computational method for a class of switched system optimal control problems. *IEEE Transactions on Automatic Control*, 54(10):2455–2460, 2009.